Biosensors and Bioelectronics 89 (2017) 735–742

Contents lists available at ScienceDirect

Biosensors and Bioelectronics

journal homepage: www.elsevier.com/locate/bios

Carbon-based nanocomposites with aptamer-templated silver nanoclusters for the highly sensitive and selective detection of platelet-derived growth factor

Zhihong Zhang*, Chuanpan Guo, Shuai Zhang, Linghao He, Minghua Wang, Donglai Peng, Junfeng Tian, Shaoming Fang

Henan Provincial Key Laboratory of Surface and Interface Science, Zhengzhou University of Light Industry, No. 136, Science Avenue, Zhengzhou 450001, China

ARTICLE INFO

Keywords:
Silver nanoclusters
Carbon-based nanocomposites
PDGF-BB
Electrochemical biosensor
Electrochemical impedance spectra

ABSTRACT

We synthesized two kinds of carbon-based nanocomposites of silver nanoclusters (AgNCs). An aptamer for targeted platelet-derived growth factor-BB (PDGF-BB) detection was used as the organic phase to produce AgNCs@Apt, three dimensional reduced graphene oxide@AgNCs@Aptamer (3D-rGO@AgNCs@Apt), and graphene quantum dots@AgNCs@Aptamer (GQD@AgNCs@Apt) nanocomposites. The formation mechanism of the developed nanocomposites was described by detailed characterizations of their chemical and crystal structures. Subsequently, the as-synthesized nanoclusters containing aptamer strands were applied as the sensitive layers to fabricate a novel electrochemical aptasensor for the detection of PDGF-BB, which may be directly used to determine the target protein. Electrochemical impedance spectra showed that the developed 3D-rGO@AgNCs@Apt-based biosensor exhibited the highest sensitivity for PDGF-BB detection among three kinds of fabricated aptasensors, with an extremely low detection limit of 0.82 pg mL^{-1}. In addition, the 3D-rGO@AgNCs@Apt-based biosensor showed high selectivity, stability, and applicability for the detection of PDGF-BB. This finding indicated that the AgNC-based nanocomposites prepared by a one-step method could be used as an electrochemical biosensor for various detection procedures in the biomedical field.

1. Introduction

As a widely used biomarker for hepatic fibrosis, liver cancer, and gastrointestinal stromal tumors, platelet-derived growth factor (PDGF) has been implicated in the pathogenesis of angiogenesis in these tumor types (Wang et al., 2007). PDGF is a growth factor protein found in human platelets and has three isoforms: PDGF-AB, PDGF-AA, and PDGF-BB (Babu et al., 2013). Among them, PDGF-BB, an important cytokinein serum, is a protein marker for cancer diagnosis and directly involved in many cell transformation processes, such as tumor growth and progression (Hannink and Donoghue, 1989). PDGF-BB is close to some appalling diseases, such as atherosclerosis, fibrosis and often over-expressed inhuman malignant tumors serving as an indicator for tumor angiogenesis (Betsholtz et al., 1984). Therefore, cognition and quantification of PDGF-BB are particularly significant in biomedical fields. With the increasing demands of proteomic strategies for the clinical diagnosis and therapeutic analysis, the development of accurate, highly selective, sensitive, and facile detection of cancer-related proteins receives significant attention (Bezuidenhout et al., 2007; Liang et al., 2013; Wang et al., 2015). To date, various commonly available methods, such as enzyme-linked immunosorbent assay (Gersuk et al., 1989), fluorescence immunoassay (Huang et al., 2005), and chemiluminescence immunoassay (Huang et al., 2008), were developed for PDGF-BB detection. However, these methods are expensive, time consuming, and labor-intensive (Liu et al., 2015b). In the past few decades, electrochemical techniques have been receiving considerable interest for the detection of small biomolecules owing to their high sensitivity, rapid response, and low expense. For example, Fu's groups explored an enzyme-mediated direct electrochemistry for sensitive detection of PDGF. This proposed aptasensor shows a relatively low detection limit of 1.7 pM (Deng et al., 2013).

Aptamers are single-stranded DNA or RNA selected via an in vitro evolution process of systemic evolution of ligands through exponential enrichment (Yu et al., 2012). Aptamers have many advantages, such as a high level of both specificity and affinity, easy synthesis and storage, and flexibility in labeling at a desired site without loss of activity. Thus,

* Corresponding author.
E-mail address: mainzhh@163.com (Z. Zhang).

http://dx.doi.org/10.1016/j.bios.2016.11.019
Received 5 August 2016; Received in revised form 2 November 2016; Accepted 3 November 2016
Available online 12 November 2016

aptamers are more suitable for protein detection than antibodies (Huang et al., 2008). Recently, combining the distinct properties of aptamers with various transducers, multiple sensing strategies, such as fluorescence (Lan et al., 2010), surface-enhanced Raman spectroscopy (Wang et al., 2010), microgravimetry (Freeman et al., 2009), quartz crystal microbalance (QCM) (Yao et al., 2009), electrochemiluminescence (Zhuo et al., 2015), surface plasmon resonance (SPR) (Chen et al., 2015), and electrochemistry (Li et al., 2015), have been developed. Among these, electrochemical aptasensors based on the specificity of aptamer-target recognition have received particular attention because of their high sensitivity and selectivity, simplicity, and economy (Liu et al., 2015b). Various nanomaterials have been applied for signal amplification, including gold nanoparticles (Gong et al., 2015), carbon nanostructures (Zhong et al., 2015), and quantum dots (Lim et al., 2015), to achieve highly sensitive electrochemical aptasensors. Nevertheless, nanomaterial application has many disadvantages, such as complicated procedures, high expenses, and poor reproducibility and quantification, particularly for the complex samples (Borm et al., 2006). Aptamer immobilization is one of the key steps that can be addressed to improve the biosensor response, thermostability, and long-term stability. Covalent immobilization of the aptamer could improve the amount of bound protein. Therefore, simple aptasensors for ultrasensitive and convenient detection of proteins are still an urgent demand.

DNA sequences can be changed and modulated easily; thus, DNA has recently emerged as an attractive template to fabricate inorganic nanoparticles, which possess distinct physical and chemical properties in optics, magnetic, electronic, and catalysis. In particular, DNA-directed silver nanocluster (AgNC) syntheses have been thoroughly investigated, and the strongly emissive AgNCs@DNA show a wide range of potential applications, specifically in biosensing. These materials may have some advantages, such as ease of synthesis, desirable photophysical properties, and a smaller size than quantum dots. They also allow flexible modification with aptamers or other recognition elements when they are used in biosensing or bioimaging fields. To date, AgNCs are widely used in the aspects of light scattering (Anand et al., 2012), fluorescence (Zhang et al., 2014b), chemiluminescence (Deng and Ju, 2013), and electroluminescence (Li et al., 2014) for their excellent optical properties. Despite the excellent properties found in AgNCs, some of their other significant properties, such as the electrocatalytic activity, are considered with little attention. Moreover, AgNCs are rarely used in the field of electrochemistry.

Carbon-based materials are the current most widely used nanomaterials for the fabrication of electrodes because of their semiconductive behavior and high porosity; these materials are also suitable for protein detection (Sarma et al., 2009). To the best of our knowledge, no report is available regarding the one-step synthesis of the carbon-related AgNCs@Apt and its application on the electrochemical biosensor for sensitive protein detection. Compared with previous colorimetric and fluorescence reports, the current strategy presents two advantages. First, unlike other sensitive layer of electrochemical aptasensors, the binding of probe aptamer with the nanomaterials is combined with the inorganic nanoclusters. Second, the application of carbon-based nanomaterials in AgNCs@Apt could improve the electrochemical performances and lead to high sensitivity of the developed electrochemical sensing system (Scheme 1).

2. Experimental section

2.1. Materials

Silver nitrate ($AgNO_3$) and sodium borohydride ($NaBH_4$) was obtained from Aladdin Chemical Reagent Co. Ltd. (Shanghai, China). Sodium hydroxide was purchased from Tianjin ZhiYuan Chemical Reagen Co. Ltd. PDGF-BB, bovine serum albumin (BSA), human serum, and mouse immunoglobulin G (IgG) were obtained from Solarbio Bioengineering Ltd. Company (Beijing, China). Aptamer was obtained from SBS Genetech Co., Ltd. (Beijing, China), and the sequence was: 5′-CAG GCT ACG GCA CGT AGA GCA TCA CCA TGA TCC TG-3′. Thrombin from human plasma was obtained from Sigma-Aldrich Co. Ltd. The whole reagents were of analytical grade, and all solutions were prepared with Milli-Q ultrapure water (≥18.2 MΩ·cm).

The buffer was 0.1 M phosphate-buffered saline (PBS, pH 7.4). The aptamer stock solution (100 μm) was prepared in above PBS and stored at −4 °C. PDGF-BB and other protein stock solutions (1 mg mL^{-1}) were prepared by dissolving the proteins in PBS buffer (100 mM, pH 7.4) and further being diluted with the reaction buffer to obtain the desired concentration. The actual sample was obtained from the diluted human serum containing different PDGF-BB concentrations. The electrochemical behaviors of the modified electrodes were evaluated through cyclic voltammetry (CV), electrochemical impedance spectroscopy (EIS), and differential pulse voltammetry (DPV) in 5 mM $K_3[Fe(CN)_6]$ of PBS solution containing 1 M KCl and 0.14 M NaCl.

2.2. Preparation of AgNCs@Apt, 3D-rGO@AgNCs@Apt, and GQD@AgNCs@Apt composites

The preparation procedure of three dimensional reduced graphene oxide (3D-rGO) was same as our previous work (Yang et al., 2015). Furthermore, graphene quantum dots (GQD) was obtained from 3D-rGO via oxidation with a mixture of concentrated HNO_3 and H_2SO_4 under stirring for 24 h and ultrasonication for 24 h at room temperature. Finally, the solution was dialyzed thrice with a dialysis bag (molecular weight: 8000 Da). Typically, 100 μL of 0.1 mg mL^{-1} $AgNO_3$ solution was added to 500 μL of aptamer (1 μm) in PBS with vigorous stirring at room temperature for 5 min. The mixture was kept in the dark at 0 ℃ for 3 h. Subsequently, about 100 μL of 2.3 mg mL^{-1} $NaBH_4$ was dropwise added to the above solution until the solution turned from colorless to brown, which indicated the formation of various amounts of clusters. As a result, the AgNCs@Apt composite was obtained. As for the preparation of the 3D-rGO@AgNCs@Apt and GQD@AgNCs@Apt composites, 0.01 mg of 3D-rGO and 1 mL GQD were added into the mixture of $AgNO_3$ and aptamer solution for 3 h, separately, according to the same procedure with the preparation of AgNCs@Apt composite.

2.3. Fabrication of electrochemical biosensors based on AgNCs@Apt, 3D-rGO@AgNCs@Apt, and GQD@AgNCs@Apt composites

Prior to modification, the surface of gold electrode was washed with piranha solution (H_2SO_4:H_2O_2=7:3) and rinsed in ethanol and water under ultrasonication for 5 min. The electrochemical biosensor was prepared through dropping 10 μL of pre-prepared AgNCs@Apt, 3D-rGO@AgNCs@Apt, or GQD@AgNCs@Apt onto the surface of the gold electrode. Briefly, the modified gold electrode was immersed in different concentrations of PDGF-BB for 2 h during electrochemical measurement.

2.4. Characterizations

X-ray photoelectron spectroscopy (XPS) analysis was obtained from an AXIS HIS 165 spectrometer (Kratos Analytical, Manchester, UK) with a monochromatized Al KR x-ray source (1486.71 eV photons). The surface morphology was determined using a high-resolution transmission electron microscope (TEM, JEOL JEM-2100) with a field emission gun of 200 kV. UV–vis spectra were obtained through a computer-controlled UV–vis spectrometer (TU-1201, Beijing Instrument Company).

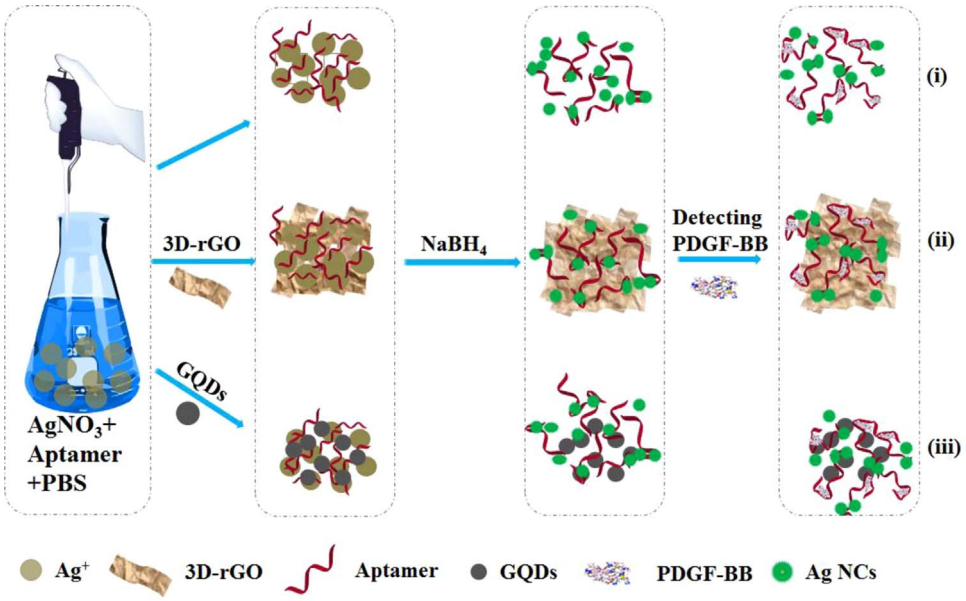

Scheme 1. Schematic diagram of preparing the electrochemical biosensors based on nanocomposites of aptamer-templated silver nanoclusters (AgNCs) (i) and carbon-related nanomaterials (ii) and (iii) for detecting platelet-derived growth factor BB (PDGF-BB).

2.5. Electrochemical measurements

Electrochemical measurements were carried out on an electrochemical workstation (CHI 660B, CH Instruments). A conventional three-electrode system was employed, which consisted of the modified gold electrode with a diameter of Ø3 mm as the working electrode, a Ag/AgCl (saturated KCl) electrode as reference electrode, and a platinum slide as counter-electrode. CV and EIS were both performed at room temperature. The scan range of CV was from −0.2 to 0.8 V, the scan rate was 0.1 V/s, and sensitivity was 10^{-5} A/V. For EIS, 5 mM $[Fe(CN)_6]^{3-/4-}$ with 1 M KCl and 140 mM NaCl in PBS (pH 7.4) was employed as the electrolyte. The spectra were recorded by applying a bias potential of 0.22 V versus Ag/AgCl (saturated KCl) and 5 mV amplitude in the frequency ranging from 0.01Hz to 100 kHz. Furthermore, the spectra were analyzed using Zview2 software, which utilized a nonlinear least squares fit to determine the parameters of the elements in an equivalent circuit. The Randles equivalent circuit consisted of solution resistance (R_s), charge-transfer resistance (R_{ct}), constant-phase element, and Warburg impedance (W_o) (as shown inset in Fig. S1). Fig. S1 shows the R_{ct} and ΔR_{ct} ($\Delta R_{ct} = R_{ct,2} - R_{ct,1}$) values for the aptamer binding capacity and response signals of the PDGF-BB. Each measurement was repeated for at least thrice.

3. Results and discussion

3.1. Chemical components of as-prepared AgNC-related nanocomposites

XPS analysis was performed to identify the elements present in the as-prepared nanoclusters. The XPS survey scan spectra for three samples are summarized in Fig. S2. The substantially strong signals of C 1*s*, N 1*s*, and O 1*s* were observed, whereas weak signals of P 2*p* and Ag 3*d* coexisted. Table S1 presents that the atom% of C 1*s* in AgNCs@Apt (46.98%) was higher than that of 3D-rGO@AgNCs@Apt (46.32%) and GQD@AgNCs@Apt (23.94%). The other elemental contents (N 1*s* and Ag 3*d*) were relatively low. Among them, the contents of Ag 3*d* in the three kinds of nanoclusters were low at 0.33%, 0.05%, and 0.71%. The high-resolution XPS spectra of C 1*s*, N 1*s*, and Ag 3*d* region of the as-prepared nanoclusters are summarized in Fig. 1. In high-resolution XPS spectra of the C 1 *s* region (Fig. 1**a**1, **b**1, and **c**1), four peaks at ~284.6, ~285.7, ~286.8, and ~288.1 eV corresponded to C–C/C–H, C–N, C–O, C=O, and/or N–C=O groups, respectively. Among them, C–N or N–C=O was attributed to the presence of the oligonucleotide strands in the nanocomposites; C–O and C=O could be resulted from 3D-rGO and GQD. However, functional groups of phenyl and O–C=O were still observed in the high-resolution XPS spectrum of the C 1 *s* in the 3D-rGO@AgNCs@Apt nanocluster, which were present in the 3D-rGO. These peaks were absent in the GQD@AgNCs@Apt nanocomposite. The high-resolution XPS spectra of the N 1 *s* regions of the developed nanoclusters (Fig. 1**a**2, **b**2 and **c**2) were the C–N/N–H at ~399.3 eV and =N– at ~397.8 eV, which are originated from aptamer. As shown in Fig. 1**a**3, **b**3, and **c**3, the high-resolution XPS spectra of the Ag 3*d* regions can be fitted into two parts at ~367.54 and ~373.3 eV, which further confirmed that the oxidation state of Ag was zero.

3.2. Characterizations of as-prepared AgNC-related nanocomposites

The formation and properties of AgNCs@Apt, 3D-rGO@AgNCs@Apt, and GQD@AgNCs@Apt were characterized using UV–vis absorption spectroscopy, fluorescent spectroscopy, and TEM. Fig. S3 shows the UV–vis spectra for the formation of Ag NPs on aptamer strands. The results showed a similar trend for three samples. A characteristic absorption band at 260 nm in the absorption spectrum was attributed to aromatic base molecules in DNA (Rajendra et al., 2004). In addition to the DNA peak, a new peak appeared at a wavelength of 444 nm, which corresponded to the SPR of the Ag NCs (Bukasov and Shumaker-Parry, 2009). Ag NCs are well-known for their fluorescent properties; thus, the three samples were subjected to fluorescence spectroscopic characterization. As indicated by Fig. S3, the excitation and emission peaks of AgNCs@Apt nanocomposite were observed at 399.8 and 529 nm, whereas they were referred to 392 and 485 nm for GQD@AgNCs@Apt nanocomposite, respectively. These peaks were different from those reported in other works. Normally, cytosine-rich oligonucleotides are used for the templated synthesis of AgNCs because of Ag(I)-mediated base pairs comprising entirely natural bases, namely, cytosine–Ag(I)–cytosine (Chen et al., 2014; Yuan et al., 2014), cytosine–Ag(I)–adenine (Liu et al., 2015a), and cytosine–Ag(I)–thymine (Funai et al., 2014). However, in the present work, the aptamer strands with random base sequence were used, which caused the weak interaction between aptamer strands and Ag^+ ions and further affected the reduction ability of Ag^+ to Ag atoms. Consequently, the number of

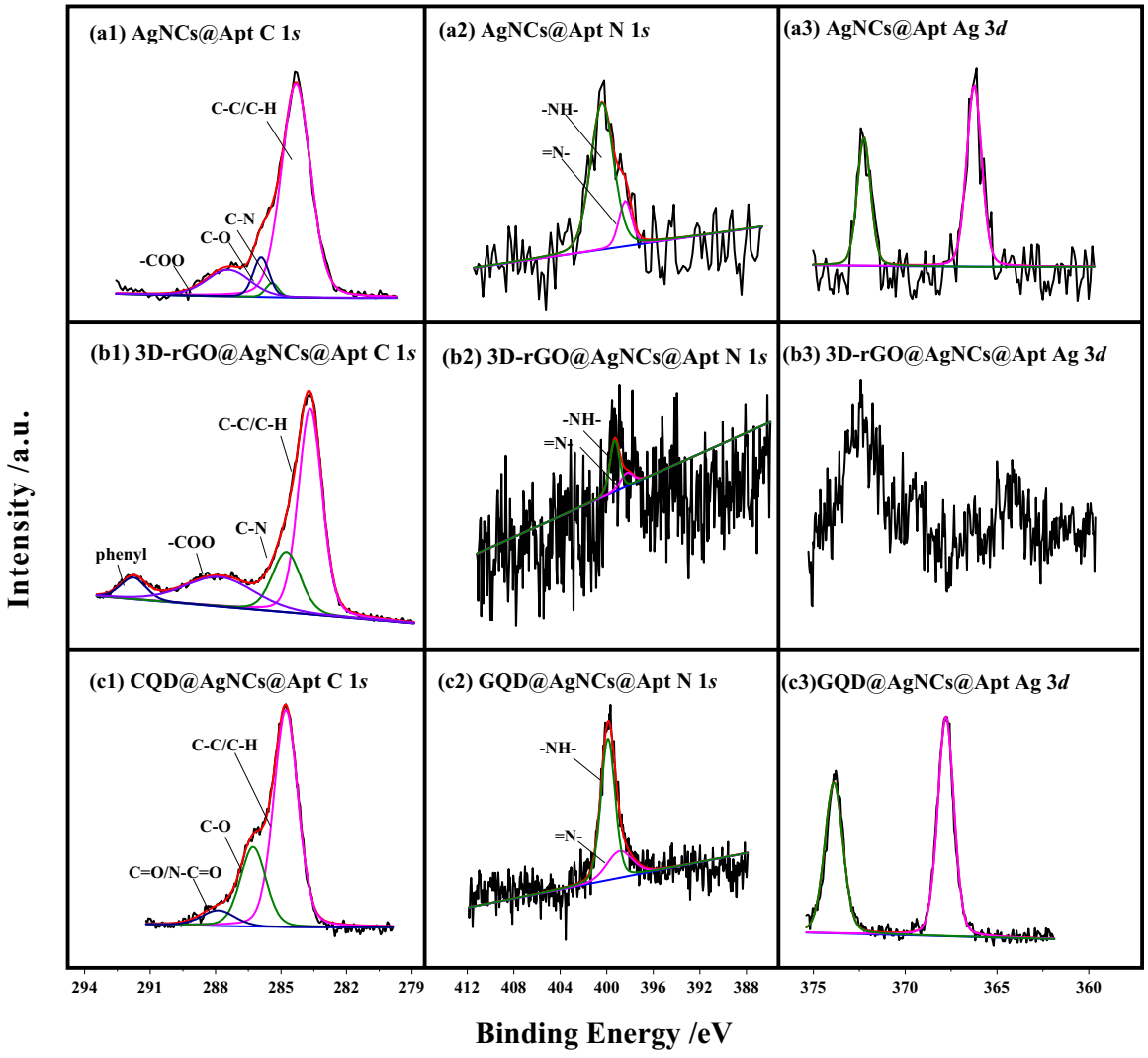

Fig. 1. C 1*s*, N 1*s*, and Ag 3*d* core-level XPS spectra of (a) AgNCs@Apt, (b) 3D-rGO@AgNCs@Apt, and (c) GQD@AgNCs@Apt nanocomposites.

Ag atoms that formed Ag NCs is less than the reported papers (Sharma et al., 2011; Zhang et al., 2014a). The excitation and emission peaks of the 3D-rGO@AgNCs@Apt nanocomposite were 200 and 329 nm. As discussed in other works, the fluorescence of nanoclusters can be quenched in the presence of 3D-rGO, thereby resulting in the less fluorescence intensity or shift of peak positions (Lu et al., 2016).

Whether AgNCs were obtained despite the lack of significant fluorescence was investigated. In case of AgNCs@Apt nanocomposite, the TEM images (Fig. 2**a**1) showed that nanoparticles (> 10 nm diameter) and nanoclusters (< 10 nm diameter) were formed. The crystallinity of Ag NCs was not considerably clear because of the lacking clear lattice of AgNCs (Fig. 2**a**2). Nevertheless, for 3D-rGO@AgNCs@Apt nanocomposite, AgNCs were distributed homogeneously onto 3D-rGO nanosheets with the approximate size of 2–3 nm (Fig. 2**b**1 and **b**2). The AgNC and GQD composites caused the formation of some large nanoparticles with a multidispersed size ranging from 1 to 7 nm (Fig. 2**c**1 and **c**2). Accordingly, AgNCs can be well stabilized with aptamer strands in the presence of 3D-rGO in comparison with the three samples.

3.3. Electrochemical performances of as-prepared AgNC-related nanocomposites

During the determination of PDGF-BB using the developed sensors based on three kinds of nanocomposites, the variations of electrochemical performances were characterized through EIS, DPV, and CV. Among them, EIS has been regarded as a sensitive method to probe the electron transfer (R_{ct}) of an interface between the electrolyte solution and modified electrode. In the EIS spectroscopy, the semicircle portion observed at high frequencies corresponds to the electron transfer limiting process, and the interfacial R_{ct} can be directly determined through the diameter of the semicircle (Li et al., 2007). For the AgNCs@Apt nanocomposite-modified electrode (Fig. 3**a**), the R_{ct} for AE was approximately 0.09 kohm (curve a). When AgNCs@Apt nanocomposite was modified on AE (curve b), the R_{ct} value substantially increased to 0.28 kohm, which suggested that AgNCs@Apt film reduced the electron transfer and electrochemical activity of the gold electrode. In addition to the AgNCs within the composite, the organic phase of aptamer strands was predominant. Consequently, the presence of oligonucleotide molecules can block the electron transfer at the interface between the electrolytes and electrode, thereby leading to the increase of the R_{ct} value (Miao et al., 2009). The composite electrode was applied to detect PDGF-BB. The R_{ct} value further increased to 0.35 kohm, which indicated the covering of PDGF-BB onto the electrode surface to further prevent the electron transfer (Degefa and Kwak, 2008).

When the three kinds of composite electrodes modified with AgNCs@Apt (Fig. 3**a**), 3D-rGO@AgNCs@Apt (Fig. 3**b**), and GQD@AgNCs@Apt (Fig. 3**c**) nanocomposites were compared, a similar trend, i.e., the continuous increase in R_{ct} values during the whole procedures

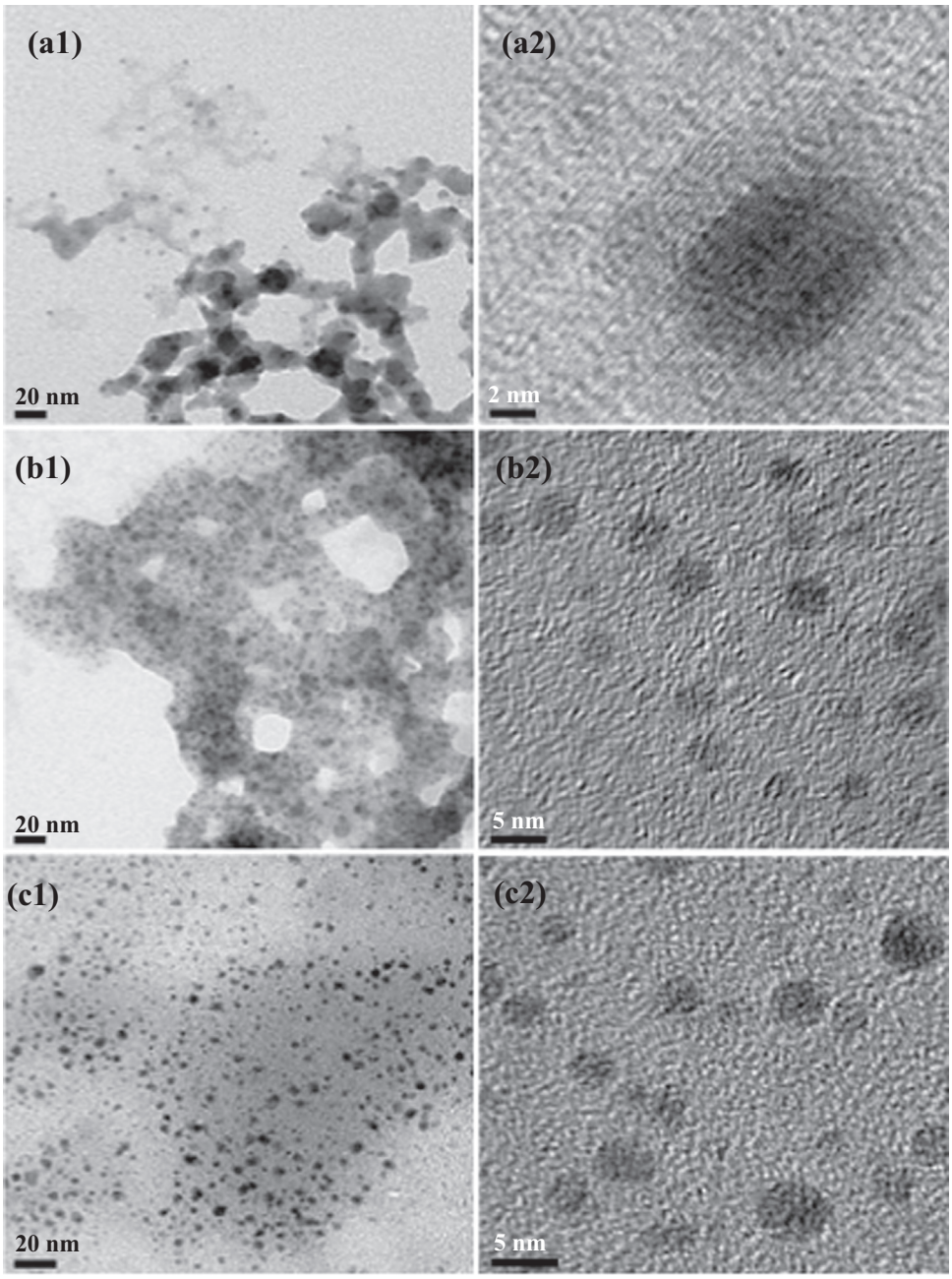

Fig. 2. Transmission electron microscope images of (a) AgNCs@Apt, (b) 3D-rGO@AgNCs@Apt, and (c) GQD@ AgNCs@Apt nanocomposites.

of the PDGF-BB detection, was observed. To display the efficiency of the determination using the different developed sensing strategies, Fig. 3**d** shows the ΔR_{ct} values obtained from each step for the three samples. The results demonstrated that the ΔR_{ct} value of the GQD@ AgNCs@Apt-modified AE was the highest, thereby suggesting its relatively weak electrochemical performances. However, after the PDGF-BB detection, the 3D-rGO@AgNCs@Apt-based aptasensor with the highest ΔR_{ct} exhibited the most desirable biosensing ability. This observation can be explained with the homogeneous distribution of the Ag NCs and high intensity of aptamer strands, which can improve the binding points with protein molecules. Furthermore, DPV measurements were also performed to determine each step of the detection of PDGF-BB, of which the experiment procedure is same as EIS method. As shown in Fig. S4a-4c, the bare gold electrode shows the largest current peak (I_p). Since the coverage of the nanomaterials coated on the bare gold electrode with relatively low electrochemical activity inhibits the access of electrons, leading to low electron-transfer efficiency of the system, the I_p values of the modified electrode with AgNCs@Apt, 3D-rGO@AgNCs@Apt, and GQD@AgNCs@Apt decrease. It demonstrates that the I_p values further decreases after the PDGF-BB detection, indicating that the binding of PDGF-BB with aptamer strands inhibits the access of electrons to the modified surface. The ΔI values of each step during the detection of PDGF-BB for three kinds of aptasensors were summarized in Fig. S4d. It illustrates that the similar results were obtained with those of EIS measurements.

Similarly, the CVs of different modified electrodes were conducted in 5 mM $[Fe(CN)_6]^{3-/4-}$ with 1 M KCl and 0.14 M NaCl in PBS (Fig. S5). Three samples exhibited a same trend: electrode materials presented a smaller current response than that of the AE. This difference in current response could be caused by that electrode materials blocked the electron transfer between the electrodes and solution. When the PDGF-BB was assembled on the above aptamer-modified AE, a decreased current was obtained. The PDGF-BB could hinder the electron transfer after binding with the aptamer strands.

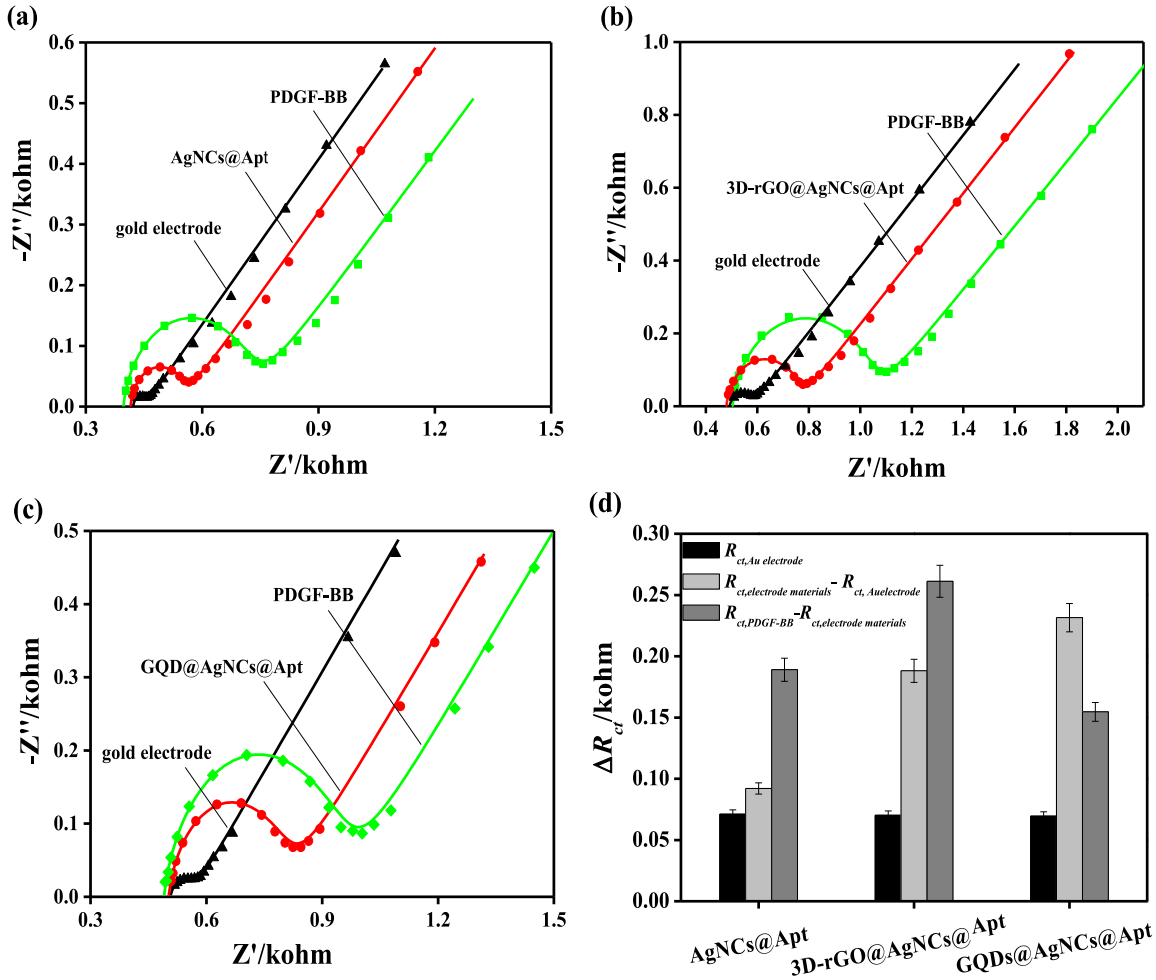

Fig. 3. Electrochemical impedance spectroscopy (EIS) Nyquist plots of the (a) AgNCs@Apt, (b)3D-rGO@AgNCs@Apt, and (c) GQD@AgNCs@Apt nanocomposite-modified Au electrode and composite electrodes after 0.001 ng mL^{-1} PDGF-BB detection. (d) Variation in the charge-transfer resistance (R_{ct}) values for each stage in the detection of PDGF-BB. Simulated R_{ct} values were measured using the developed electrochemical aptasensors, in which AgNCs@Apt, 3D-rGO@AgNCs@Apt, and GQD@AgNCs@Apt nanocomposites were used as the sensitive layers.

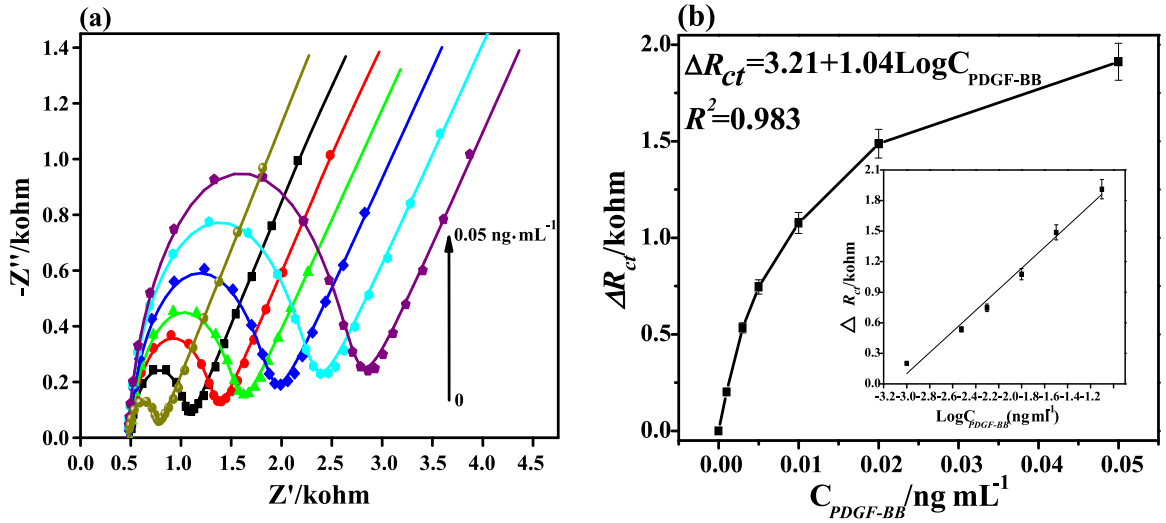

Fig. 4. (a) EIS Nyquist plots for the detection of different concentrations of PDGF-BB using the developed electrochemical biosensor based on 3D-rGO@AgNCs@Apt nanocomposite. The concentrations are 0, 0.001, 0.003, 0.005, 0.01, 0.02, and 0.05 ng mL^{-1}. (b) The linear fit plots ΔR_{ct} as function of the logarithm of the PDGF-BB concentrations. Error bar represents the standard deviation of three parallel experiments.

Table 1
Comparison between the proposed method and other reported electrochemical aptasensors for the PDGF-BB detection.

Electrode of materials	Technique	Linear range	LOD	References
Aptamer-based sensor	DPV	50 pM – 10 nM	50 pM	(Lai et al. 2007)
Layered molybdenum selenide-graphene composites	EIS	0.0001 – 1 nM	20 fM	(Huang et al. 2016)
Poly(diallyldimethylammonium chloride)-protected graphene-gold nanoparticles composite	DPV	0.005 – 60 nM	1.7 pM	(Deng et al. 2013)
Leaf-like VS_2 nanosheets	DPV	0.001 – 1.0 nM	0.4 pM	(Liu et al. 2015c)
Klenow Fragment polymerase	DPV	4 pM – 4.69 nM	1.8 pM	(Yu et al. 2012)
Electrochemical immunosensor with an aptamer-primed	Square wave voltammetry (SWV)	1.6 – 16.1 nM	0.58 nM	(Huang et al. 2008)
MoS_2@carbon aerogel composites	DPV	0.001 – 10 nM	0.3 pM	(Fang et al. 2015)
3D-rGO@AgNCs@aptamer	EIS	32.3 fM–1.61 pM	26.5 fM	This work

The results were in good agreement with the EIS measurements.

3.4. Sensitivity of the developed electrochemical biosensors

To evaluate the analytical performance of the designed aptasensors, EIS experiments were carried out by adding different concentrations of PDGF-BB to the sensor to examine whether the R_{ct} value could be used for quantification (Fig. 4**a**). Additionally, to renew the developed biosensor after EIS measurement for each concentration, it was rinsed with PBS and Milli-Q water successively, following by being dried in N_2 atmosphere. In case of the fabricated aptasensor based on 3D-rGO@AgNCs@Apt nanocomposite, the R_{ct} values increased significantly with increasing concentration of target PDGF-BB protein. The PDGF-BB target protein can be quantitatively detected as low as 1 pg mL^{-1}.

As shown in the inset of Fig. 4**b**, the calibration plots displayed a good linear relationship between the peak currents and PBGF-BB concentrations ranging from 1 pg mL^{-1} to 0.05 ng mL^{-1} with a regression equation of ΔR_{ct} =3.21+1.04 $LogC_{PDGF\text{-}BB}$ and a correlation coefficient (R^2) of 0.983. The limit of detection (LOD) was 0.82 pg mL^{-1} at a signal-to-noise ratio of 3. The same approach was used in the determination of the LODs for the PDGF-BB detection of the developed aptasensors based on AgNCs@Apt and GQD@AgNCs@Apt nanocomposites, as shown in Figs. S6 and S7, respectively. Regression equations of ΔR_{ct} =8.11+5.31 $LogC_{PDGF\text{-}BB}$ with a correlation coefficient (R^2) of 0.998 and ΔR_{ct} =2.83+1.1 $LogC_{PDGF\text{-}BB}$ with a correlation coefficient (R^2) of 0.992 were observed. As such, the similar LODs of 1.14 and 3.50 pg mL^{-1} were obtained for AgNCs@Apt and GQD@AgNCs@Apt nanocomposites, respectively. Moreover, the LODs of the developed aptasensors were also determined by DPV measurements (Fig. S8). The LODs for AgNCs@Apt-, 3D-rGO@AgNCs@Apt-, and GQD@AgNCs@Apt-based aptasensor are calculated to be 5.10, 1.34 and 8.12 pg mL^{-1} for the determination of PDGF-BB (S/N=3), respectively. It is clear that the sensitivities resulted from EIS and DPV were very close and kept in the same order of magnitude. Compared with the reported electrochemical methods listed in Table 1 for the PDGF-BB detection, the proposed aptasensor showed significant improvement in the detection limit of PDGF-BB.

3.5. Selectivity, stability, and repeatability of the developed aptasensors

About 1 ng mL^{-1} BSA, thrombin, Lys, and IgG in PBS, which may interfere with the detection of target protein, and 0.02 ng mL^{-1} PDGF-BB were examined to evaluate the selectivity of the fabricated aptasensor based on 3D-rGO@AgNCs@Apt nanocomposite. The results showed that only PDGF-BB produced the remarkable signal amplification (Fig. S9). The error bars represented average standard errors for three measurements. The experimental results demonstrated that the established assay method exhibited specific response to target protein, as expected.

The reusability of the aptasensor is considerably important for practical application, such as clinical diagnoses and biological monitoring, which is dependent on the stability and regeneration ability of the biosensor. In the present work, when the fabricated aptasensor based on 3D-rGO@AgNCs@Apt nanocomposite was stored at 4 °C for 10 days and subsequently measured with EIS in $[Fe(CN)_6]^{3-/4-}$, the change in the R_{ct} response was only 3.7% compared with the initial test, which indicated the good stability of the biosensor. The developed aptasensor was regenerated by incubating it in 10% sodium dodecyl sulfate (SDS) solution for 10 mins and then being washed carefully with PBS (Wang et al., 2009). The procedure was repeated 10 times continuously (Fig. S10). It is clear that the response signal to the same concentration of PDGF-BB can be recovered.

3.6. Feasibility of the developed biosensor in complex sample

Whether the constructed aptasensor could work directly in human blood serum was studied to investigate the feasibility of the developed DNA biosensor in complex matrixes. Ten standards with various PDGF-BB concentrations were spiked into the blank serum samples, and the PDGF-BB contents were assayed using the electrochemical aptasensor. The results are listed in Table S2. The recoveries were within the range from 93.3% to 108%, which indicated that the electrochemical aptasensor presented good recovery. The aptasensor, which was distinguished with its convenient miniaturization for low assay cost, high sensitivity, and absence of complicated and expensive array detectors, showed suitability for the point-of-care testing. Therefore, the developed aptasensor can be potential tool for convenient detection of PDGF-BB in human specimens in clinical laboratory diagnosis.

4. Conclusions

Novel AgNCs containing carbon nanomaterials and aptamer were synthesized via one-step method. Thus, the developed electrochemical biosensors based on AgNCs@Apt, 3D-rGO@AgNCs@Apt, and GQDs@AgNCs@Apt were applied for the sensitive detection of PGDF-BB. Carbon-based AgNCs@Apt nanocomposites exhibited good biocompatibility, high functionality, and specificity for protein detection; thus, the related fabricated electrochemical biosensors of AgNCs@Apt, 3D-rGO@AgNCs@Apt, and GQDs@AgNCs@Apt exhibited considerably low detection limit of 1.14, 0.82, and 3.50 pg mL^{-1}, respectively. The results indicated that the presence of 3D-rGO can improve the affinity of the PDGF-BB binding. Therefore, the 3D-rGO@AgNCs@Apt-based biosensor showed high selectivity, stability, and applicability for the detection of PDGF-BB.

Acknowledgment

This work was supported by Programs for the National Natural Science Foundation of China (NSFC: Account No. 21601161) and Innovative Team of Henan Province (2014).

Appendix A. Supplementary material

Supplementary data associated with this article can be found in the online version at doi:10.1016/j.bios.2016.11.019.

References

Anand, U., Ghosh, S., Mukherjee, S., 2012. J. Phys. Chem. Lett. 3 (23), 3605–3609.
Babu, E., Singaravadivel, S., Manojkumar, P., Krishnasamy, S., Rajagopal, S., 2013. Anal. Bioanal. Chem. 405 (21), 6891–6895.
Betsholtz, C., Westermark, B., Ek, B., Heldin, C.-H., 1984. Cell 39 (3), 447–457.
Bezuidenhout, L., Bracher, M., Davison, G., Zilla, P., Davies, N., 2007. J. Leukoc. Biol. 81 (6), 1496–1503.
Borm, P.J., Robbins, D., Haubold, S., Kuhlbusch, T., Fissan, H., Donaldson, K., Schins, R., Stone, V., Kreyling, W., Lademann, J., 2006. Part. Fibre Toxicol. 3 (1), 1.
Bukasov, R., Shumaker-Parry, J.S., 2009. Anal. Chem. 81 (11), 4531–4535.
Chen, H., Qi, F., Zhou, H., Jia, S., Gao, Y., Koh, K., Yin, Y., 2015. Sens. Actuat. B-Chem. 212, 505–511.
Chen, J., Zhang, X., Cai, S., Wu, D., Chen, M., Wang, S., Zhang, J., 2014. Biosens. Bioelectron. 57, 226–231.
Degefa, T.H., Kwak, J., 2008. Anal. Chim. Acta 613 (2), 163–168.
Deng, K., Xiang, Y., Zhang, L., Chen, Q., Fu, W., 2013. Anal. Chim. Acta 759, 61–65.
Deng, S., Ju, H., 2013. Analyst 138 (1), 43–61.
Fang, L.X., Huang, K.J., Liu, Y., 2015. Biosens. Bioelectron. 71, 171–178.
Freeman, R., Li, Y., Tel-Vered, R., Sharon, E., Elbaz, J., Willner, I., 2009. Analyst 134 (4), 653–656.
Funai, T., Nakamura, J., Miyazaki, Y., Kiriu, R., Nakagawa, O., Wada, S., Ono, A., Urata, H., 2014. Angew. Chem. Int. Ed. 53 (26), 6624–6627.
Gersuk, G.M., Carmel, R., Pattengale, P.K., 1989. Blood 74 (7), 2330–2334.
Gong, Y., Chen, X., Lu, Y., Yang, W., 2015. Biosens. Bioelectron. 66, 392–398.
Hannink, M., Donoghue, D.J., 1989. BBA-Rev. Cancer 989 (1), 1–10.
Huang, C.C., Huang, Y.F., Cao, Z., Tan, W., Chang, H.T., 2005. Anal. Chem. 77 (17), 5735–5741.
Huang, K.J., Shuai, H.L., Zhang, J.Z., 2016. Biosens. Bioelectron. 77, 69–75.
Huang, Y., Nie, X.M., Gan, S.L., Jiang, J.H., Shen, G.L., Yu, R.Q., 2008. Anal. Biochem. 382 (1), 16–22.
Lai, R.Y., Plaxco, K.W., Heeger, A.J., 2007. Anal. Chem. 79 (1), 229–233.
Lan, G.Y., Huang, C.C., Chang, H.T., 2010. Chem. Commun. 46 (8), 1257–1259.
Li, A., Yang, F., Ma, Y., Yang, X., 2007. Biosens. Bioelectron. 22 (8), 1716–1722.
Li, M., Wang, Y., Zhang, Y., Yu, J., Ge, S., Yan, M., 2014. Biosens. Bioelectron. 59, 307–313.
Li, X.M., Wang, L.L., Luo, J., Wei, Q.L., 2015. Biosens. Bioelectron. 65, 245–250.
Liang, J., Wei, R., He, S., Liu, Y., Guo, L., Li, L., 2013. Analyst 138 (6), 1726–1732.
Lim, C.S., Hola, K., Ambrosi, A., Zboril, R., Pumera, M., 2015. Electrochem. Commun. 52, 75–79.
Liu, H., Wang, Y., Zhang, L., Shao, Y., Zheng, B., 2015a. Mater. Lett. 139, 265–267.
Liu, S., Kang, M., Yan, F., Peng, D., Yang, Y., He, L., Wang, M., Fang, S., Zhang, Z., 2015b. Electrochim. Acta 160, 64–73.
Liu, X., Shuai, H.L., Huang, K.J., 2015c. Anal. Methods 7 (19), 8277–8284.
Lu, Y.-W., Hu, Y., Huang, C., Cheng, S., Xu, C.X., Luo, P.F., Cheng, J.G., Jiang, Y., 2016. Appl. Phys. Lett. 108 (15), 153113.
Miao, P., Liu, L., Nie, Y., Li, G., 2009. Biosens. Bioelectron. 24 (11), 3347–3351.
Rajendra, J., Baxendale, M., Dit Rap, L.G., Rodger, A., 2004. J. Am. Chem. Soc. 126 (36), 11182–11188.
Sarma, A.K., Vatsyayan, P., Goswami, P., Minteer, S.D., 2009. Biosens. Bioelectron. 24 (8), 2313–2322.
Sharma, J., Yeh, H.C., Yoo, H., Werner, J.H., Martinez, J.S., 2011. Chem. Commun. 47 (8), 2294–2296.
Wang, G., Zhu, Y., Chen, L., Zhang, X., 2015. Biosens. Bioelectron. 63, 552–557.
Wang, J., Meng, W., Zheng, X.F., Liu, S.L., Li, G.X., 2009. Biosens. Bioelectron. 24 (6), 1598–1602.
Wang, Y., Lee, K., Irudayaraj, J., 2010. J. Phys. Chem. C 114 (39), 16122–16128.
Wang, Z., Kong, D., Banerjee, S., Li, Y., Adsay, N.V., Abbruzzese, J., Sarkar, F.H., 2007. Cancer Res. 67 (23), 11377–11385.
Yang, Y., Kang, M., Fang, S., Wang, M., He, L., Zhao, J., Zhang, H., Zhang, Z., 2015. Sens. Actuat. B-Chem. 214, 63–69.
Yao, C., Qi, Y., Zhao, Y., Xiang, Y., Chen, Q., Fu, W., 2009. Biosens. Bioelectron. 24 (8), 2499–2503.
Yu, T., Li, J., Liu, Q., Cheng, W., Zhang, D., Ju, H., Ding, S., 2012. Int. J. Electrochem. Sci. 7, 8533–8542.
Yuan, Y., Li, W., Liu, Z., Nie, Z., Huang, Y., Yao, S., 2014. Biosens. Bioelectron. 61, 321–327.
Zhang, K., Wang, K., Zhu, X., Zhang, J., Xu, L., Huang, B., Xie, M., 2014a. Chem. Commun. 50 (2), 180–182.
Zhang, L., Liang, R.P., Xiao, S.J., Bai, J.M., Zheng, L.L., Zhan, L., Zhao, X.J., Qiu, J.D., Huang, C.Z., 2014b. Talanta 118, 339–347.
Zhong, A., Luo, X., Chen, L., Wei, S., Liang, Y., Li, X., 2015. Microchim. Acta 182 (5–6), 1197–1204.
Zhuo, B., Li, Y., Huang, X., Lin, Y., Chen, Y., Gao, W., 2015. Sens. Actuat. B-Chem. 208, 518–524.